Title
Sleep Drive Is Encoded by Neural Plastic Changes in a Dedicated Circuit.

Journal
Cell, 165(6)

Authors
Liu, Sha
Tabuchi, Masashi
Wu, Mark
et al.

Publication Date
2016-06-02

DOI
10.1016/j.cell.2016.04.013

Peer reviewed

HHS Public Access

Author manuscript

Cell. Author manuscript; available in PMC 2017 June 02.

Published in final edited form as:

Cell. 2016 June 2; 165(6): 1347–1360. doi:10.1016/j.cell.2016.04.013.

Sleep drive is encoded by neural plastic changes in a dedicated circuit

Sha Liu[#1], **Qili Liu**[#1], **Masashi Tabuchi**[1], and **Mark N. Wu**[1,2,*]

[1]Department of Neurology, Johns Hopkins University, Baltimore, MD 21287

[2]Department of Neuroscience, Johns Hopkins University, Baltimore, MD 21287

[#] These authors contributed equally to this work.

Summary

Prolonged wakefulness leads to an increased pressure for sleep, but how this homeostatic drive is generated and subsequently persists is unclear. Here, from a neural circuit screen in *Drosophila*, we identify a subset of ellipsoid body (EB) neurons whose activation generates sleep drive. Patch-clamp analysis indicates these EB neurons are highly sensitive to sleep loss, switching from spiking to burst-firing modes. Functional imaging and translational profiling experiments reveal that elevated sleep need triggers reversible increases in cytosolic Ca^{2+} levels, NMDA receptor expression, and structural markers of synaptic strength, suggesting these EB neurons undergo "sleep need"-dependent plasticity. Strikingly, the synaptic plasticity of these EB neurons is both necessary and sufficient for generating sleep drive, indicating that sleep pressure is encoded by plastic changes within this circuit. These studies define an integrator circuit for sleep homeostasis and provide a mechanism explaining the generation and persistence of sleep drive.

The concept of homeostasis for maintaining stability of an animal's "internal milieu" was first articulated more than 150 years ago (Cannon, 1929). These principles are also relevant for motivated behaviors that are regulated by homeostatic drive (Berridge, 2004). Sleep is an archetypal example of such a behavior—prolonged wakefulness increases sleep drive (sleep pressure), resulting in an increase in sleep amount and/or depth ("sleep rebound") (Borbely, 1982). However, despite intense scrutiny for more than a century, the mechanisms underlying this process and the nature of sleep drive itself remain unclear. In addition, homeostatic regulation of motivated behaviors, such as feeding or sleeping, typically occurs over a long period (Berridge, 2004; Borbely, 1982); substantial accumulation of sleep drive in many animals takes hours of wakefulness, and is often maintained for hours even after

---

[*]Correspondence to: (; Email: marknwu@jhmi.edu)

Additional methods and experimental details are available in the Supplemental Experimental Procedures.

Author contributions

S.L. and Q.L. performed behavioral experiments and immunostaining. S.L. performed functional imaging and TRAP experiments. M.T. conducted electrophysiological analyses. S.L., Q.L., M.T., and M.N.W. designed and analyzed experiments. S.L. and M.N.W. primarily wrote the manuscript with input from all authors.

sleep is initiated (Daan et al., 1984; Huber et al., 2000; Huber et al., 2004). Therefore, unraveling the processes encoding sleep drive requires an understanding of both how sleep drive is generated and how it persists.

Most work on sleep drive has centered on extracellular sleep regulatory substances (SRS), such as adenosine, whose levels rise with prolonged wakefulness in specific regions of the brain ("somnogen model") (Brown et al., 2012). These SRS have traditionally been proposed to act on dedicated circuits that directly promote sleep or wakefulness in mammals, such as the ventrolateral preoptic nucleus (VLPO), median preoptic nucleus (MnPO), or specific acetylcholinergic nuclei (Methippara et al., 2005; Porkka-Heiskanen et al., 1997). In this model, sleep drive is generated by the accumulation of these SRS, or "somnogens," in the extracellular space (Brown et al., 2012). However, the half-lives of these SRS are typically much shorter (minutes) (Jonzon and Fredholm, 1985; Pettipher et al., 2007) than the timecourse for dissipating sleep pressure (hours), raising the possibility that, rather than directly encoding sleep pressure, these SRS act as effectors of sleep drive to promote sleep (Benington and Heller, 1995).

From an engineering perspective, homeostatic systems require 3 components: a) a sensor that periodically samples the state variable, b) an integrator that processes this information to determine homeostatic drive, and c) an effector that responds to this drive by directly manipulating the state variables (Enderle and Bronzino, 2012). Thus, general design principles predict that, for sleep homeostasis, central circuits should exist that both encode the amount of sleep pressure and play a crucial role in mediating the perdurance of such sleep drive. However, such circuits have not been previously found.

Here, from a large-scale forward screen of neuronal driver lines in *Drosophila*, we identify a neural circuit capable of generating sleep drive. Remarkably, activation of this circuit induces sleep pressure and persistent sleep behavior, even in fully rested animals. Conversely, neuronal silencing experiments reveal a specific requirement for this circuit in sleep homeostasis. Patch-clamp analysis demonstrates that this circuit is highly sensitive to changes in sleep need. Importantly, we find that intracellular Ca^{2+} levels and the synaptic strength of this circuit not only tightly correlate with, but are also able to specifically manipulate, the level of homeostatic sleep drive. Finally, cell-specific translational profiling reveals significant upregulation of NMDA receptors in this circuit following sleep deprivation, and we show that this upregulation is a key mechanism mediating "sleep need"-dependent plastic changes in this circuit and, ultimately, the generation of sleep drive. Together, our data suggest a model whereby sleep pressure is encoded by plastic changes within a dedicated homeostatic integrator circuit, providing a mechanistic explanation for the generation and persistence of sleep drive.

Results

Identification of a neuronal circuit that induces sleep drive

Drosophila is an established genetic model system for studying sleep, and shares similar sleep-regulatory mechanisms with vertebrates (Cirelli, 2009; Sehgal and Mignot, 2011). For example, sleep in fruit flies is regulated by both the circadian clock and homeostatic sleep

drive (Donlea et al., 2014; Kunst et al., 2014; Liu et al., 2014), and specific monoaminergic nuclei directly promote arousal and can do so by inhibiting specific sleep-promoting circuits (Liu et al., 2012; Ueno et al., 2012). Thus, to study neural circuit mechanisms regulating sleep and wakefulness, we conducted a large-scale neuronal driver screen in *Drosophila*. 505 Gal4 drivers that together cover most neuropils of the fly brain were selected from the Rubin/Janelia Farm collection (Jenett et al., 2012) based upon the sparseness of their expression patterns. Using these drivers, we conditionally activated different subsets of neurons with the heat-activated cation channel dTrpA1 (Hamada et al., 2008) for 12 hrs during the night, and measured sleep amount during that night and during the following day after cessation of dTrpA1 activation (Figure 1). Sleep amount during and after dTrpA1 activation generally displayed an inverse relationship reflecting sleep homeostasis (Figure 1A). For example, wake-promoting drivers such as *R52B10-Gal4* tended to induce significant "sleep rebound" after dTrpA1 activation had ended (Figures 1A-1D and S1A). From this screen, we identified multiple sleep-promoting drivers that express in the ExFl2 neurons, including *R72G06-Gal4* and *R12G09-Gal4* (Figures 1A-1D, S1C, and S1D). These neurons have recently been shown to act as a sleep "effector" circuit, whose activation directly induces sleep in *Drosophila* (Donlea et al., 2014; Donlea et al., 2011), thus validating our approach.

To our surprise, we found several lines that markedly violated the inverse relationship between sleep amount during and after dTrpA1 activation (Figures 1A-1D, S1A-S1B, S1ES1G). These drivers strongly induced sleep after dTrpA1 activation had ceased, but tended to also increase sleep during activation. Analysis of the expression patterns of these 8 drivers indicated that a specific group of ellipsoid body (EB) ring neurons--the R2 neurons--was illuminated by the majority of these drivers (Figures 1E, 1F, and S1E). We first focused on one of these drivers, *R69F08-Gal4*, since it had the most specific expression pattern in the central brain (Figure 1G). The inactivity observed following dTrpA1 activation did not persist the following day, suggesting that it was not secondary to neural injury (Figure S1B). To further confirm that the daytime inactivity observed following heat activation of *R69F08-Gal4>UAS-dTrpA1* animals was due to sleep and not paralysis or locomotor impairment, we performed a series of control experiments. This quiescence behavior was reversible and associated with an increased arousal threshold (Figure 1H), suggesting that these animals were asleep and not paralyzed. Waking activity of these *R69F08-Gal4>UAS-dTrpA1* flies after being fully aroused (>2g stimulation for 5 sec) at ZT2 (Zeitgeber time 2) was similar to control flies, indicating these flies did not have locomotor impairment following dTrpA1 activation (Figure S1H). To ensure that the flies were truly inactive, and not simply grooming or feeding, we performed video analysis of *R69F08-Gal4>UAS-dTrpA1* flies and manually scored their behavior for the 2 hrs after dTrpA1 activation. As expected, we found that these flies spent the majority of the 2 hrs immobile and only a minor fraction of their time grooming or feeding (immobile: 80.0% ± 1.9%; grooming: 9.6% ± 1.2%; feeding: 3.7% ± 0.8%, n=15). The sleep behavior elicited by activation of the R2 cells led to deeper sleep compared to controls (Figure 1H). Moreover, after being briefly awakened at ZT2 (2 hours after cessation of dTrpA1 activation), these *R69F08-Gal4>UAS-dTrpA1* flies were more likely to return to sleep, and to do so more quickly (Figure 1I), further indicating increased sleep propensity after dTrpA1 activation. Similar data were obtained for an

independent driver (*R58H05-Gal4*) that also drives expression in these R2 neurons (Figures 1C, 1D, 1H, and 1I). Because increases in sleep amount and depth are hallmarks of increased homeostatic sleep drive (Borbely, 1982; Huber et al., 2004), and because these phenotypes occur following cessation of neural activation, these data strongly suggest that activating R2 neurons genetically induces persistent sleep drive.

R2 neurons are required for generating homeostatic sleep drive

To address whether the R2 circuit is also required for generating homeostatic sleep drive, we assessed whether silencing these neurons impaired sleep recovery following sleep deprivation. Expression of tetanus toxin (TNT) (Sweeney et al., 1995), which inhibits neurotransmitter release, in R2 neurons using 3 restricted Gal4 drivers (*R69F08-Gal4*, *R58H05-Gal4*, or *R30G03-Gal4*) markedly reduced "rebound sleep" following mechanical sleep deprivation (Figures 2A and 2B). In addition, sleep depth following sleep deprivation was reduced, compared to control animals (Figure 2C). In contrast, when TNT was expressed using 2 drivers that appeared to induce sleep pressure in our screen, but do not contain R2 neurons (*R35D04-Gal4* and *R59B03-Gal4*, Figure S1E), sleep rebound was not significantly affected (Figure 2B). *R27G06-Gal4* was not tested in this assay, since it was lethal in combination with *UAS-TNT*. Importantly, inactivation of these R2 ring neurons did not significantly affect baseline sleep, indicating a specific role for these neurons in the homeostatic regulation of sleep (Figures S2A-C). Together with our neural activation data, these findings indicate that this R2 circuit is both necessary and sufficient for homeostatic regulation of sleep.

The R2 circuit acts upstream of a sleep-promoting circuit to regulate sleep homeostasis

If the R2 circuit encodes physiological sleep drive, one would expect it to act upstream of a sleep "effector" circuit. In flies, recent data indicate that the ExFl2 neurons, which project to the dorsal fan-shaped body, act as an "effector" circuit that directly promotes sleep in response to increases in sleep drive (Donlea et al., 2014). Therefore, we asked whether the R2 circuit we identified acts upstream of the ExFl2 circuit in the homeostatic regulation of sleep (Figure 2D). To address this question, we blocked neurotransmitter release from the ExFl2 neurons using the LexA/LexAop system (Lai and Lee, 2006) and assessed sleep following activation of R2 neurons using the Gal4/UAS system. The *R72G06-LexA* line drives expression in the ExFl2 neurons, and we confirmed that thermogenetic activation of these neurons using dTrpA1 promoted sleep (Figures S2D-S2F), similar to *R72G06-Gal4* (Figure 1) and other previously described ExFl2 drivers (Donlea et al., 2011). As before, nighttime activation of the R2 neurons using the *R69F08-Gal4* driver (*wt>LexAop-TNT*; *R69F08-Gal4>UAS-dTrpA1*) led to "rebound"-like sleep during the following day. This phenotype was largely reduced when ExFl2 neurotransmission was simultaneously inhibited (*R72G06-LexA>LexAop-TNT*; *R69F08-Gal4>UAS-dTrpA1)* (Figures 2E and 2F), consistent with the notion that the R2 neurons promote sleep via the ExFl2 neurons. To examine potential functional connectivity between the R2 and ExFl2 neurons, we used 2 binary systems to simultaneously express ATP-gated P2X2 receptors (Lima and Miesenbock, 2005) in R2 neurons and GCaMP6s in ExFl2 neurons. As shown in Figure 2G, activation of the R2 neurons by application of ATP induced a substantial increase in GCaMP signal in ExFl2 neurons in experimental flies, but not control flies lacking P2X2 receptors in

R2 neurons. Together, these data strongly suggest that the R2 neurons act upstream of the ExFl2 neurons in the homeostatic regulation of sleep.

The activity and excitability of R2 neurons is enhanced following prolonged wakefulness

The preceding data suggest that sleep drive is generated within the R2 circuit. To address whether the functional properties of these neurons are altered with sleep need, we performed patch-clamp recordings from these neurons at different timepoints and following sleep deprivation (Figure 3A). Because these neurons have not previously been characterized electrophysiologically, we first tried different recording configurations. We found that these R2 cells were amenable to perforated patch-clamp recordings using beta-escin (Sarantopoulos et al., 2004), which was preferred because of the importance of intracellular Ca^{2+} in these neurons (see below). Two classes of neurons within the R2 cluster were identified: one class exhibited spontaneous action potential (AP) firing, while the other appeared to be non-spiking in nature. We focused on the spiking cells, because they constituted the majority (~92%) of neurons in the R2 cluster. Under baseline conditions, we recorded from 2 timepoints: ZT0-ZT2 (when sleep pressure should be low) and ZT13-ZT15 (when sleep pressure should be moderately elevated). We found that the spontaneous AP firing rate of the R2 neurons was increased ~3-fold at ZT13-ZT15, compared to ZT0-ZT2. Moreover, following sleep deprivation, the spontaneous AP firing rate further increased, compared to rested flies assessed at ZT0-ZT2 (Figures 3B and 3D). Strikingly, bursting events were seen in the majority (75%) of recordings from sleep-deprived flies, but never seen under baseline conditions at ZT0-ZT2 or ZT13-ZT15 (Figures 3C and 3D), suggesting a switch to a “potentiated” state after sleep loss. Furthermore, evoked AP firing rates were higher at most (for ZT13-ZT15) and all (for sleep-deprived) measured depolarizing currents vs those at ZT0-ZT2 (Figures 3E and 3F). The resting membrane potential of R2 neurons was also more depolarized in animals following sleep deprivation, while input resistance was not altered (Figures S3A and S3B). Together, these data indicate that the activity and excitability of the R2 circuit increase under conditions of greater sleep need and that these neurons exhibit burst firing specifically following sleep deprivation.

Structural plastic changes in the R2 circuit correlate with sleep pressure

The switch to a “burst” firing pattern in R2 neurons of sleep-deprived animals suggests not only a change in their intrinsic cellular properties, but also raises the possibility of plastic changes within these cells (Moore et al., 2009). In support of this concept, some of the electrophysiological data in Figure 3 were obtained 1-2 hrs after the end of sleep deprivation, suggesting persistence of this phenotype. Given that plastic changes in synaptic strength could be an elegant mechanism for encoding the build-up and persistence of sleep drive, we investigated whether structural markers of synaptic strength changed in R2 cells following sleep deprivation. To do this, we used the STaR (Synaptic Tagging with Recombination) system (Chen et al., 2014), which enables labeling of active zones specifically within a defined circuit, by tagging native Bruchpilot (BRP) in a FLP/FRT dependent manner. Changes in BRP levels are a key mechanism underlying activity-dependent plasticity in adult neurons (Sugie et al., 2015), and changes in synaptic structure, and both number and size of active zones in particular, are generally associated with changes in synaptic strength (Holderith et al., 2012; Weyhersmuller et al., 2011). Two hours after

mechanical sleep deprivation had ended, BRP signal in the R2 ring structure was significantly increased in sleep-deprived flies compared to rested control flies (Figures 4A-4C), and this greater BRP signal was due to increases in both the number and size of BRP puncta in the R2 ring (Figure 4D). Similar data were obtained using an independent thermogenetic method for inducing sleep deprivation (Figures S3E and S3F). When sleep drive is dissipated following 24 hours of recovery sleep, the increased BRP signal is lowered to levels seen in rested control animals (Figures 4B and 4C), demonstrating that these changes are reversible. In contrast, increased BRP signal following sleep deprivation was not observed in other neurons in the brain, including antennal lobe local interneurons, ExFl2 neurons, and R3 ring neurons, suggesting specificity to this phenotype (Figures 4B, 4C, S3C, and S3D). Although prior work found an increase in BRP in antennal lobes following sleep deprivation (Gilestro et al., 2009), the entire antennal lobe structure was assessed using anti-BRP antibodies in that study, compared to our examination of specific antennal lobe interneurons using the STaR system. Together, these data argue that levels of molecular markers of synaptic strength in the R2 neurons correlate with levels of sleep drive and suggest that “sleep need”-dependent plastic changes in the R2 circuit may be relevant for generating homeostatic sleep drive.

Cytosolic Ca^{2+} levels in R2 neurons signify levels of sleep drive

Experimental evidence and theoretical models suggest a crucial role for intracellular Ca^{2+} levels in driving neural plasticity (Berridge, 1998; O'Leary et al., 2014). Therefore, we next asked whether intracellular Ca^{2+} levels in the R2 neurons also correlate with different levels of sleep drive. To measure Ca^{2+} levels over the course of multiple hours, we used the CaLexA (Calcium-dependent nuclear import of LexA) system (Masuyama et al., 2012). This system drives expression of GFP in response to sustained increases in cytosolic Ca^{2+}. We used a strong R2 driver (*R30G03-Gal4*) to drive CaLexA in R2 neurons, and also examined the signal in other neurons labeled by this driver as an internal control. After 24 hrs of mechanical sleep deprivation (Figure 5A), the GFP signal in the R2 ring structure was substantially higher in sleep-deprived flies compared to control flies, while the signal intensity in other neuropil structures, such as the Fan-shaped body, was unchanged (Figures 5B and 5C). Similar data were obtained using another R2 neuron-containing driver (*R58H05-Gal4*) (Figure 5D). These data suggest that Ca^{2+} levels are specifically increased within R2 neurons following sleep deprivation. To rule out the possibility that the increased CaLexA signal in R2 neurons was caused solely by mechanical stimulation and not a change in sleep pressure *per se*, we mechanically sleep-deprived flies for only 12 hours during the subjective day (when flies are mostly awake) vs subjective night (when flies are generally asleep), and assessed CaLexA signal in the R2 neurons. When *R30G03-Gal4>CaLexA* animals were mechanically sleep-deprived during the subjective nighttime, the CaLexA signal in the R2 neurons was significantly increased compared to controls, whereas it was similar to controls with daytime sleep deprivation (Figures S4A-S4D). These data suggest that the increased CaLexA signal is induced by increased sleep drive and not by mechanical stimulation alone. It is well-described that very young animals in multiple species exhibit increased sleep amount and depth, compared to adults (Frank and Heller, 1997; Roffwarg et al., 1966). In *Drosophila*, a recent study demonstrated that young flies have significantly increased sleep drive compared to older animals (Kayser et al., 2014). Consistent with this

notion, we found that the CaLexA signal in R2 neurons was dramatically higher in very young animals compared to older animals (Figures 5E-5H). Together, these imaging data reveal that Ca^{2+} levels in R2 neurons are increased under conditions associated with markedly increased sleep drive: following sleep deprivation or in very young animals.

We next examined whether Ca^{2+} levels in these R2 neurons varied naturally with sleep pressure, in the absence of sleep deprivation. We used the genetically-encoded Ca^{2+} reporter *UAS-myrGCaMP5G* (Melom and Littleton, 2013) to monitor real-time Ca^{2+} levels in the R2 ring structure. Ca^{2+} levels were measured at ZT0 (low sleep drive), ZT12 (moderate sleep drive), ZT24 (low sleep drive), and ZT24 following 12 hrs of sleep deprivation (high sleep drive) (Figure 5I). We found that basal Ca^{2+} levels in the R2 ring were higher in the early night (ZT12) compared to the morning (ZT0 and ZT24) (Figures 5J and 5K). This difference was attributable to changes in sleep drive and not circadian time, because Ca^{2+} levels in the R2 ring were further increased at ZT24 after 12 hrs of sleep deprivation during the night (Figures 5J and 5K). A similar increase in GCaMP signal was found using an independent thermogenetic method for inducing sleep deprivation or using an independent GCaMP line, indicating that this effect is not dependent on mechanical shaking or a specific GCaMP (Figures S4E-H). In contrast, this increase was not observed in neuronal structures nearby to the R2 ring (i.e., R3 and R4m rings), indicating it does not occur broadly in all ellipsoid body rings (Figure S4I). Thus, our data indicate that Ca^{2+} levels in the R2 neurons correlate with varying levels of sleep drive in a scalable manner, consistent with a potential role for neural plastic changes in this circuit mediating sleep homeostasis.

Manipulation of intracellular Ca^{2+} levels adjusts synaptic strength in R2 neurons and alters sleep drive

We hypothesized that these variations in intracellular Ca^{2+} levels are functionally important for the sleep need-dependent structural plasticity seen in R2 neurons. If so, altering intracellular Ca^{2+} levels in these neurons would provide a means for testing whether manipulating neural plasticity impacts sleep homeostasis. Previous work has shown that reduction of Inositol-triphosphate receptor (IP3R) activity impairs elevation of cytosolic Ca^{2+} levels and Ca^{2+}-dependent plasticity (Berridge, 1998). Therefore, we drove expression of 2 different *UAS-IP3R-RNAi* transgenes (Murmu et al., 2010) in the R2 neurons and examined the effects on intracellular Ca^{2+} levels and structural plasticity. We first confirmed that both RNAi transgenes were effective in reducing *IP3R* transcript (Figure S5A). Knockdown of IP3R in R2 neurons using either RNAi transgene largely suppressed the increased intracellular Ca^{2+} seen in these cells following sleep deprivation (Figure 6A), in contrast to an unrelated control RNAi line (Figure S5C). As shown in Figure 6B, blocking the rise of intracellular Ca^{2+} levels in R2 neurons with either *IP3R-RNAi* line significantly impaired the increases in number and size of BRP puncta seen in these neurons following sleep deprivation. To address the effects of these manipulations on sleep homeostasis, we drove expression of the two *IP3R-RNAi* transgenes in the R2 cells and measured sleep rebound in animals following sleep deprivation. Importantly, knockdown of IP3R in R2 neurons using either RNAi transgene caused a significant reduction in recovery sleep compared to controls (Figure 6C). Furthermore, knockdown of IP3R in R2 neurons using either *IP3R-RNAi* line did not affect baseline sleep, indicating a specific effect on sleep

homeostasis (Figure S5B). Given that some rebound sleep persists in the absence of increases in cytosolic Ca^{2+} and BRP in R2 neurons (Figures 6A-C), there may be additional mechanisms encoding homeostatic sleep drive. Together, these data suggest that Ca^{2+}-dependent plastic changes in R2 neurons are specifically required for proper homeostatic regulation of sleep.

In order to conditionally increase intracellular Ca^{2+} levels within the R2 circuit, we elevated the temperature from ZT0-ZT1 (instead of activating dTrpA1 from ZT12-ZT24 as done previously) for animals expressing dTrpA1 in the R2 neurons. Remarkably, this protocol led to an increase in number and size of BRP puncta in these cells, similar to that seen following sleep deprivation (Figure 6D), suggesting an increase in synaptic strength. Moreover, as little as 30 minute activation of dTrpA1 in the R2 circuit induced a significant increase in sleep mimicking “rebound sleep” following the temperature elevation, despite the animals being fully rested (Figures 6E and 6F and Figure S5D). Thus, these data suggest that Ca^{2+}-dependent changes in synaptic strength of the R2 circuit are not only necessary, but also sufficient for encoding sleep drive.

NMDA receptor signaling in R2 neurons is required for encoding homeostatic sleep drive

Although Ca^{2+} signaling is crucial for neural plasticity, it is also involved in diverse cellular signaling pathways (Clapham, 2007). Thus, to further identify and test additional mechanisms underlying plasticity-dependent generation of homeostatic sleep drive, we performed cell-specific translational profiling experiments in the R2 neurons. Because the utility of this technique greatly depends on using an exquisitely specific driver, we used the split-Gal4 system (Luan et al., 2006) to generate a driver almost exclusively containing the 16 R2 neurons (Figure 7A). As expected, activation of this R2-Split-Gal4 driver leads to a persistent increase in sleep following cessation of the stimulus, as seen with other R2 Gal4 drivers (Figures S6A-S6D).

We used this R2-Split-Gal4 driver to express the EGFP-L10a fusion protein in the R2 circuit, and performed Translating Ribosome Affinity Purification (TRAP) experiments (Huang et al., 2013) to isolate actively translating transcripts from these 16 neurons. As expected, RTPCR demonstrated marked enrichment of GFP transcript in the R2 TRAP samples, whereas mRNA of the glial-specific marker *repo* was essentially undetectable in the same samples (Figure 7B). We extracted R2 neuron-specific mRNA from sleep-deprived and rested control flies and examined the levels of plasticity-related transcripts in R2 cells using qPCR. Interestingly, levels of a NMDA receptor subunit (*dNR1*) were markedly (~7-fold) and specifically increased in the R2 neurons, but not broadly in all neurons (Figure 7C). NMDA receptors in flies consist of two subunits: dNR1 and dNR2 (Xia et al., 2005). To confirm an associated increase in NMDA receptor protein levels, we performed immunostaining experiments using anti-dNR2 antisera, which revealed a significant increase in dNR2 levels in R2 neurons following sleep deprivation (Figures S6E and S6F). To address whether NMDA receptors are required for the structural plasticity in R2 neurons induced by sleep loss, we performed RNAi knockdown experiments using 2 different RNAi lines targeting *dNR1* or *dNR2* (Wu et al., 2007) and then examined BRP puncta using the STaR system. We first confirmed that these RNAi lines were effective at reducing *dNR1* and *dNR2*

levels, respectively (Figures S6G and S6H). Next, we found that knockdown of either dNR1 or dNR2 in R2 neurons significantly suppressed the sleep deprivation-induced increase in the number and size of BRP puncta in these cells, indicating that NMDA receptors are required in R2 neurons for "sleep need"-dependent plasticity (Figure 7D). Importantly, knockdown of either dNR1 or dNR2 in the R2 circuit significantly reduced rebound sleep after sleep deprivation (Figure 7E), but did not affect baseline sleep (Figure S6I), suggesting that NMDAR-dependent plasticity is specifically required in these neurons for generating homeostatic sleep drive. Thus, these data identify a key molecular mechanism mediating neural plastic changes in R2 neurons and demonstrate that this plasticity is required for homeostatic regulation of sleep.

Discussion

As mentioned previously, homeostatic systems are predicted to consist of "sensor," "integrator," and "effector" circuits. Activation of sleep homeostatic "effector" circuits (such as VLPO/MnPO in mammals (Saito et al., 2013) or ExFl2 neurons in flies (Donlea et al., 2014) directly induces sleep, whose persistence depends upon continued stimulation of the circuit (see also Figure 1B). In contrast, even 30 minute activation of the R2 circuit in non-sleep-deprived animals leads to a prolonged increase in sleep amount and depth following cessation of the stimulus. This phenotype indicates that activation of these neurons generates sleep drive even in fully rested animals. This unusual phenotype, coupled with our findings that these R2 neurons act upstream of the "effector" ExFl2 neurons and undergo "sleep need"-dependent plastic changes, suggest that the R2 circuit acts as a key "integrator" for sleep homeostasis.

Sleep homeostasis is thought to operate not only under conditions that provoke strong sleep drive (i.e., sleep deprivation), but also at baseline when sleep pressure gradually accumulates towards the end of the waking period (Borbely, 1982). Interestingly, although our data suggest that the R2 neurons can sense changes in sleep drive under baseline conditions (Figures 3B, 3D, 3F and 5I-5K), they are not essential for sleep amount in this situation (Figure 2A and Figures S2A-S2C). Thus, while the R2 neurons play a crucial role in the homeostatic regulation of sleep following sleep deprivation, additional mechanisms likely play a role under baseline conditions.

Our data argue that plastic changes within the R2 neural circuit generate sleep drive (Figure 7F). In this model, prolonged wakefulness leads to a sustained increase in intracellular Ca^{2+} levels in R2 neurons, which then results in greater synaptic strength as reflected by an increased number and size of active zones, and greater excitability of these neurons, as reflected by their switch to burst-firing. Thus, both synaptic and non-synaptic plasticity are induced in R2 neurons by sleep loss, which act together to markedly potentiate the activity of these cells. NMDA receptors, well-known for their role in synaptic plasticity (Malenka and Nicoll, 1993), are also upregulated in R2 neurons with sleep loss to further potentiate synaptic strength, either in concert or in parallel with the increases in intracellular Ca^{2+}. As suggested by our data (Figures S6E and S6F), NMDA receptors are shown presynaptically, which would imply strengthening of the connection between the R2 neuron and its downstream partner. However, it is also possible that NMDARs act postsynaptically. In

either case, sleep drive would be encoded by the degree of potentiation of the R2 circuit, which would then promote sleep via persistent activation of sleep "effector" neurons such as the ExFl2 cells in flies.

Our findings support an alternative model to the traditional "somnogen model" of sleep homeostasis. Rather than global sleep drive being encoded by varying levels of extracellular substances in the brain, we propose that it is encoded by Ca^{2+}- and NMDA receptor-dependent plastic changes in a dedicated neural circuit. Moreover, unlike the case for "somnogens" or SRS whose half-lives are on the order of minutes, our model provides a mechanistic explanation for the persistence of sleep drive lasting for hours following the initiation of recovery sleep. Although their brain structures are different, core circuit principles are often shared between flies and mammals (Borst and Helmstaedter, 2015; Strausfeld and Hirth, 2013). Thus, a sleep homeostatic integrator circuit, whose plastic changes encode sleep drive, may exist in mammals.

Experimental Procedures

Sleep Assays

Sleep analysis was performed as previously described (Liu et al., 2014). For sleep deprivation experiments, flies were mechanically stimulated for 5 sec per min for 12 hrs or 24 hrs using a vortexer mounting plate and multi-tube vortexer (Trikinetics). Only data from flies with a ≥95% reduction in sleep amount during deprivation, compared with baseline conditions, were analyzed. "% Recovered sleep" was calculated as the difference in sleep amount between the deprived and undisturbed control animals during the first 6 hrs following deprivation, divided by the amount of sleep lost during sleep deprivation.

BRP and CaLexA measurements

For BRP and CaLexA measurements, fly brains were whole-mount immunostained with anti-V5 or anti-GFP, respectively. Images were taken under 63x magnification, acquired at 1024×1024 pixels, and further analyzed in Fiji/ImageJ. To measure signal intensities, the sum of all pixels of a stack comprising the R2 ring or other ROIs was calculated. Background intensity adjacent to the ROI was measured and subtracted. For analysis of BRP puncta, stacks only containing R2 ring signal were extracted from the original image stacks, and number and size of BRP puncta were automatically calculated using the "3D Objects Counter" Plugin. The threshold for calculating the BRP puncta was manually determined for each stack of images, for which the largest number of BRP puncta was identified by the plugin. For CaLexA sleep deprivation experiments, 7-9 day old flies were used. To minimize effects from environmental stimulation, flies were transferred to constant darkness (DD) for 1 day prior to sleep deprivation, which was performed as described above for 12 or 24 hrs in DD.

Intracellular Ca^{2+} measurements

For intracellular Ca^{2+} level measurements, 7-9 day old *R69F08-Gal4>UAS-myrGCaMP5, UASCD4-tdTomato* or *R69F08-Gal4>UAS-GCaMP6s, UAS-CD4-tdTomato* flies were examined. GCaMP signal in the R2 ring neuropil was measured immediately (within 5 mins)

after dissection at different timepoints (ZT0 and ZT12), or following sleep deprivation. All brains were quickly dissected in AHLS, and imaged using a LSM700 confocal microscope. The R2 ring structure was located in less than 15s by fast pre-scanning of tdTomato signal (543nm). A single optical section was selected which contained the maximum area and intensity of tdTomato signal under a 63x water-immersion objective lens. GCaMP signals were recorded at 2 fps for 1 min. Average projections of all the frames in the 1 min recording were used to calculate the baseline GCaMP signal. ROIs of the R2 ring were outlined by using the tdTomato signal. Fluorescent signal from both GCaMP and tdTomato in the same ROI were each summed and normalized to the background in Fiji/ImageJ. GCaMP signal was divided by the tdTomato signal for the same ROI to correct for between-specimen variation.

Supplementary Material

Refer to Web version on PubMed Central for supplementary material.

Acknowledgements

We thank G. Rubin, T. Littleton, J. Wang, C-H. Lee, J-R. Martin, R. Jackson, C-L. Wu, and the Bloomington Stock Center for reagents. We thank C. Potter, T. Lloyd, D. O'Connor, J. Cohen, A. Kolodkin, and members of the Wu Lab for comments on the manuscript. This work was supported by NIH grants R01NS079584 (M.N.W.) and R21NS088521 (M.N.W.), NINDS Center Grant NS05027 for machine shop work, and a Burroughs-Wellcome Fund Career Award for Medical Scientists (M.N.W.).

References

Benington JH, Heller HC. Restoration of brain energy metabolism as the function of sleep. Prog. Neurobiol. 1995; 45:347–360. [PubMed: 7624482]

Berridge KC. Motivation concepts in behavioral neuroscience. Physiol. & Behav. 2004; 81:179–209. [PubMed: 15159167]

Berridge MJ. Neuronal calcium signaling. Neuron. 1998; 21:13–26. [PubMed: 9697848]

Borbely AA. A two process model of sleep regulation. Hum. Neurobiol. 1982; 1:195–204. [PubMed: 7185792]

Borst A, Helmstaedter M. Common circuit design in fly and mammalian motion vision. Nat. Neurosci. 2015; 18:1067–1076. [PubMed: 26120965]

Brown RE, Basheer R, McKenna JT, Strecker RE, McCarley RW. Control of sleep and wakefulness. Physiol. Rev. 2012; 92:1087–1187. [PubMed: 22811426]

Cannon WB. Organization for physiological homeostasis. Physiol. Rev. 1929; 9:399–431.

Chen Y, Akin O, Nern A, Tsui CY, Pecot MY, Zipursky SL. Cell-type-specific labeling of synapses in vivo through synaptic tagging with recombination. Neuron. 2014; 81:280–293. [PubMed: 24462095]

Cirelli C. The genetic and molecular regulation of sleep: from fruit flies to humans. Nat. Rev. Neurosci. 2009; 10:549–560. [PubMed: 19617891]

Clapham DE. Calcium signaling. Cell. 2007; 131:1047–1058. [PubMed: 18083096]

Daan S, Beersma DG, Borbely AA. Timing of human sleep: recovery process gated by a circadian pacemaker. Am. J. Physiol. 1984; 246:R161–183. [PubMed: 6696142]

Donlea JM, Pimentel D, Miesenbock G. Neuronal machinery of sleep homeostasis in *Drosophila*. Neuron. 2014; 81:860–872. [PubMed: 24559676]

Donlea JM, Thimgan MS, Suzuki Y, Gottschalk L, Shaw PJ. Inducing sleep by remote control facilitates memory consolidation in *Drosophila*. Science. 2011; 332:1571–1576. [PubMed: 21700877]

Enderle, JD.; Bronzino, JD. Introduction to biomedical engineering. Academic press; Burlington: 2012.

Frank MG, Heller HC. Development of REM and slow wave sleep in the rat. Am. J. Physiol. 1997; 272:R1792–1799. [PubMed: 9227592]

Gilestro GF, Tononi G, Cirelli C. Widespread changes in synaptic markers as a function of sleep and wakefulness in *Drosophila*. Science. 2009; 324:109–112. [PubMed: 19342593]

Hamada FN, Rosenzweig M, Kang K, Pulver SR, Ghezzi A, Jegla TJ, Garrity PA. An internal thermal sensor controlling temperature preference in *Drosophila*. Nature. 2008; 454:217–220. [PubMed: 18548007]

Holderith N, Lorincz A, Katona G, Rozsa B, Kulik A, Watanabe M, Nusser Z. Release probability of hippocampal glutamatergic terminals scales with the size of the active zone. Nat. Neurosci. 2012; 15:988–997. [PubMed: 22683683]

Huang Y, Ainsley JA, Reijmers LG, Jackson FR. Translational profiling of clock cells reveals circadianly synchronized protein synthesis. PLoS Biol. 2013; 11:e1001703. [PubMed: 24348200]

Huber R, Deboer T, Tobler I. Effects of sleep deprivation on sleep and sleep EEG in three mouse strains: empirical data and simulations. Brain Res. 2000; 857:8–19. [PubMed: 10700548]

Huber R, Hill SL, Holladay C, Biesiadecki M, Tononi G, Cirelli C. Sleep homeostasis in *Drosophila melanogaster*. Sleep. 2004; 27:628–639. [PubMed: 15282997]

Jenett A, Rubin GM, Ngo TT, Shepherd D, Murphy C, Dionne H, Pfeiffer BD, Cavallaro A, Hall D, Jeter J, et al. A GAL4-driver line resource for *Drosophila* neurobiology. Cell Rep. 2012; 2:991–1001. [PubMed: 23063364]

Jonzon B, Fredholm BB. Release of purines, noradrenaline, and GABA from rat hippocampal slices by field stimulation. J. Neurochem. 1985; 44:217–224. [PubMed: 3964829]

Kayser MS, Yue Z, Sehgal A. A critical period of sleep for development of courtship circuitry and behavior in *Drosophila*. Science. 2014; 344:269–274. [PubMed: 24744368]

Kunst M, Hughes ME, Raccuglia D, Felix M, Li M, Barnett G, Duah J, Nitabach MN. Calcitonin gene-related peptide neurons mediate sleep-specific circadian output in *Drosophila*. Curr. Biol. 2014; 24:2652–2664. [PubMed: 25455031]

Lai S-L, Lee T. Genetic mosaic with dual binary transcriptional systems in *Drosophila*. Nat. Neurosci. 2006; 9:703–709. [PubMed: 16582903]

Lima SQ, Miesenbock G. Remote control of behavior through genetically targeted photostimulation of neurons. Cell. 2005; 121:141–152. [PubMed: 15820685]

Liu Q, Liu S, Kodama L, Driscoll MR, Wu MN. Two dopaminergic neurons signal to the dorsal fan-shaped body to promote wakefulness in *Drosophila*. Curr. Biol. 2012; 22:2114–2123. [PubMed: 23022067]

Liu S, Lamaze A, Liu Q, Tabuchi M, Yang Y, Fowler M, Bharadwaj R, Zhang J, Bedont J, Blackshaw S, et al. WIDE AWAKE mediates the circadian timing of sleep onset. Neuron. 2014; 82:151–166. [PubMed: 24631345]

Luan H, Peabody NC, Vinson CR, White BH. Refined spatial manipulation of neuronal function by combinatorial restriction of transgene expression. Neuron. 2006; 52:425–436. [PubMed: 17088209]

Malenka RC, Nicoll RA. NMDA-receptor-dependent synaptic plasticity: multiple forms and mechanisms. Trends Neurosci. 1993; 16:521–527. [PubMed: 7509523]

Masuyama K, Zhang Y, Rao Y, Wang JW. Mapping neural circuits with activity-dependent nuclear import of a transcription factor. J. Neurogenet. 2012; 26:89–102. [PubMed: 22236090]

Melom JE, Littleton JT. Mutation of a NCKX eliminates glial microdomain calcium oscillations and enhances seizure susceptibility. J. Neurosci. 2013; 33:1169–1178. [PubMed: 23325253]

Methippara MM, Kumar S, Alam MN, Szymusiak R, McGinty D. Effects on sleep of microdialysis of adenosine A1 and A2a receptor analogs into the lateral preoptic area of rats. Am. J. Physiol. Regul. Integr Comp. Physiol. 2005; 289:R1715–1723. [PubMed: 16109808]

Moore SJ, Cooper DC, Spruston N. Plasticity of burst firing induced by synergistic activation of metabotropic glutamate and acetylcholine receptors. Neuron. 2009; 61:287–300. [PubMed: 19186170]

Murmu MS, Stinnakre J, Martin JR. Presynaptic Ca2+ stores contribute to odor-induced responses in *Drosophila* olfactory receptor neurons. J. Exp. Biol. 2010; 213:4163–4173. [PubMed: 21112997]

O'Leary T, Williams AH, Franci A, Marder E. Cell types, network homeostasis, and pathological compensation from a biologically plausible ion channel expression model. Neuron. 2014; 82:809–821. [PubMed: 24853940]

Pettipher R, Hansel TT, Armer R. Antagonism of the prostaglandin D2 receptors DP1 and CRTH2 as an approach to treat allergic diseases. Nat. Rev. Drug Discov. 2007; 6:313–325. [PubMed: 17396136]

Porkka-Heiskanen T, Strecker RE, Thakkar M, Bjorkum AA, Greene RW, McCarley RW. Adenosine: a mediator of the sleep-inducing effects of prolonged wakefulness. Science. 1997; 276:1265–1268. [PubMed: 9157887]

Roffwarg HP, Muzio JN, Dement WC. Ontogenetic development of the human sleep-dream cycle. Science. 1966; 152:604–619. [PubMed: 17779492]

Saito YC, Tsujino N, Hasegawa E, Akashi K, Abe M, Mieda M, Sakimura K, Sakurai T. GABAergic neurons in the preoptic area send direct inhibitory projections to orexin neurons. Front. Neural Circuits. 2013; 7 10.3389/fncir.2013.00192.

Sarantopoulos C, McCallum JB, Kwok WM, Hogan Q. beta-escin diminishes voltage-gated calcium current rundown in perforated patch-clamp recordings from rat primary afferent neurons. J. Neurosci. Meth. 2004; 139:61–68.

Sehgal A, Mignot E. Genetics of sleep and sleep disorders. Cell. 2011; 146:194–207. [PubMed: 21784243]

Strausfeld NJ, Hirth F. Deep homology of arthropod central complex and vertebrate basal ganglia. Science. 2013; 340:157–161. [PubMed: 23580521]

Sugie A, Hakeda-Suzuki S, Suzuki E, Silies M, Shimozono M, Mohl C, Suzuki T, Tavosanis G. Molecular Remodeling of the Presynaptic Active Zone of *Drosophila* Photoreceptors via Activity-Dependent Feedback. Neuron. 2015; 86:711–725. [PubMed: 25892303]

Sweeney ST, Broadie K, Keane J, Niemann H, O'Kane CJ. Targeted expression of tetanus toxin light chain in *Drosophila* specifically eliminates synaptic transmission and causes behavioral defects. Neuron. 1995; 14:341–351. [PubMed: 7857643]

Ueno T, Tomita J, Tanimoto H, Endo K, Ito K, Kume S, Kume K. Identification of a dopamine pathway that regulates sleep and arousal in *Drosophila*. Nat. Neurosci. 2012; 15:1516–1523. [PubMed: 23064381]

Weyhersmuller A, Hallermann S, Wagner N, Eilers J. Rapid active zone remodeling during synaptic plasticity. J. Neurosci. 2011; 31:6041–6052. [PubMed: 21508229]

Wu CL, Xia S, Fu TF, Wang H, Chen YH, Leong D, Chiang AS, Tully T. Specific requirement of NMDA receptors for long-term memory consolidation in *Drosophila* ellipsoid body. Nat. Neurosci. 2007; 10:1578–1586. [PubMed: 17982450]

Xia S, Miyashita T, Fu TF, Lin WY, Wu CL, Pyzocha L, Lin IR, Saitoe M, Tully T, Chiang AS. NMDA receptors mediate olfactory learning and memory in *Drosophila*. Curr. Biol. 2005; 15:603–615. [PubMed: 15823532]

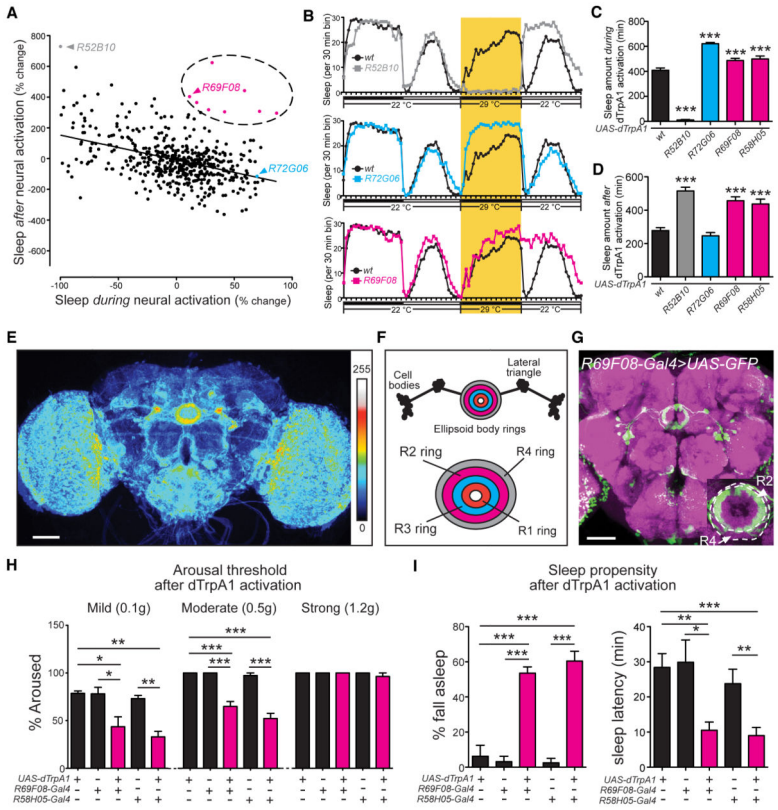

Figure 1.

Activation of R2 ring neurons induces sleep drive.

(A) Scatterplot of % change in sleep amount during and after dTrpA1 activation from 505 Gal4 lines driving expression of dTrpA1. The solid trend line shows the inverse correlation between amount of sleep during and following dTrpA1 activation. Drivers with significantly increased sleep following dTrpA1 activation, accompanied by a lack of reduced sleep during dTrpA1 activation are indicated in magenta and the dashed ellipse.

(B) Sleep profile of *wt>UAS-dTrpA1* flies (black circles, n=62) vs *R52B10-Gal4>UAS-dTrpA1* (upper panel, gray squares, n=32), *R72G06-Gal4>UAS-dTrpA1* (middle panel, cyan squares, n=32), or *R69F08-Gal4>UAS-dTrpA1* (lower panel, magenta squares, n=42). Sleep time was plotted in 30 min bins. White and black bars indicate 12 hr light and dark periods, respectively. 12 hr dTrpA1 activation at 29°C is indicated.

(C and D) Sleep amount over a 12 hr period during (**C**) and after (**D**) dTrpA1 activation for *wt>UAS-dTrpA1*, *R52B10-Gal4>UAS-dTrpA1*, *R72G06-Gal4>UAS-dTrpA1*, *R69F08-Gal4>UAS-dTrpA1*, and *R58H05-Gal4>UAS-dTrpA1* (n=24) flies. Data for all lines except *R58H05-Gal4>UAS-dTrpA1* are from the same flies as in **Figure 1B**.

(E) Heat map of the averaged GFP signal from the expression patterns of the 8 drivers indicated in magenta in **Figure 1A**. Image is presented using a “royal” look-up table, and scale is shown on the right. Scale bar denotes 100μm.

(F) Schematic showing organization of the ring neurons of the ellipsoid body. Upper panel depicts the location of cell bodies, lateral triangle (post-synaptic sites) and ellipsoid rings

(pre- and post- synaptic sites) of the ring neurons. Lower panel illustrates ellipsoid body ring anatomy: R1, R2, R3 and R4 ring structures are indicated.

(G) Whole-mount brain immunostaining of a *R69F08-Gal4>UAS-IVS-Syn21-GFP-p10* animal with anti-GFP (green) and anti-Bruchpilot (BRP, nc82, magenta). Maximal intensity projection of the central brain is shown. Scale bar denotes 100μm. Bottom right inset shows a high-magnification section of the R2 ring structure. Arrowhead indicates the R2 ring. Arrow indicates the R4 ring.

(H) Arousal threshold after dTrpA1 activation. The percentage of flies aroused by mild (0.1g), moderate (0.5g), and strong (1.2g) mechanical rotational stimuli at ZT2 after cessation of dTrpA1 activation. Data from *UAS-dTrpA1/+* (n=96 for mild, n=75 for moderate, n=64 for strong), *R69F08-Gal4/+* (n=96 for mild, n=76 for moderate, n=48 for strong), *R69F08-Gal4/UAS-dTrpA1* (n=60 for mild, n=89 for moderate, n=48 for strong), *R58H05-Gal4/+* (n=96 for mild, n=84 for moderate, n=44 for strong) and *R58H05-Gal4/UAS-dTrpA1* (n=93 for mild, n=48 for moderate, n=48 for strong) flies are shown.

(I) Sleep propensity of *UAS-dTrpA1/+*, *R69F08-Gal4/+*, *R69F08-Gal4/UAS-dTrpA1*, *R58H05-Gal4/+* and *R58H05-Gal4/UAS-dTrpA1* flies after dTrpA1 activation. % flies falling asleep within 5 mins (left panel) and sleep latency (right panel) after arousal are shown. Mean ± SEM is shown. In this and subsequent figures “*”, “**”, “***”, and “ns” denote $P<0.05$, $P<0.01$, $P<0.001$, and not significant, respectively. (See also Figure S1)

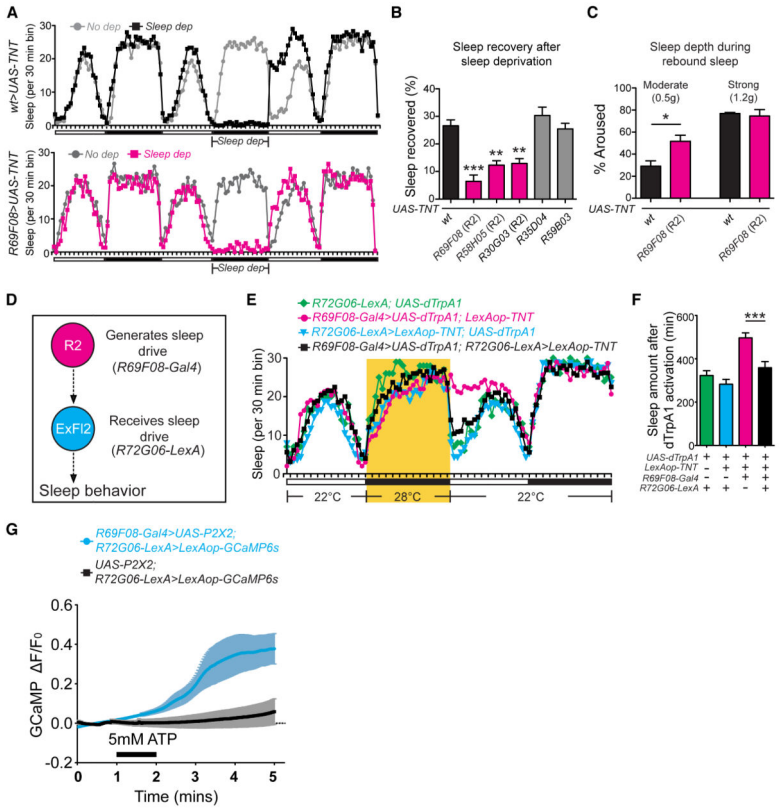

Figure 2.

R2 neurons are required and act through ExFl2 neurons to regulate sleep homeostasis.

(A) Sleep profiles of flies undergoing sleep deprivation. Sleep-deprived (black or magenta squares) and no sleep deprivation controls (gray circles) are shown for *wt>UAS-TNT* flies (upper panel, n=37 and 36 for sleep-deprived and controls, respectively) and *R69F08-Gal4>UAS-TNT* (lower panel, n=32 and 37 for sleep-deprived and controls, respectively). Sleep time plotted in 30 min bins. White and black bars indicate 12 hr light and dark periods, respectively. The 12 hr sleep deprivation period is indicated.

(B) % sleep recovered during the 6 hrs following sleep deprivation for control (*wt>UAS-TNT*), *R69F08-Gal4>UAS-TNT, R58H05-Gal4>UAS-TNT* (n=25), *R30G03-Gal4>UAS-TNT* (n=25), *R35D04-Gal4>UAS-TNT* (n=35) and *R59B03-Gal4>UAS-TNT* (n=28) flies. Data for *R69F08-Gal4>UAS-TNT* and *wt>UAS-TNT* are from the same flies as in **Figure 2A**.

(C) % aroused for *wt>UAS-TNT* (n=159 for moderate stimuli and n=128 for strong stimuli) and *R69F08-Gal4>UAS-TNT* (n=163 for moderate stimuli and n=132 for strong stimuli) flies subjected to moderate (0.5g) and strong (1.2g) mechanical rotational stimuli at ZT2 during rebound sleep. Mean ± SEM is shown.

(D) Proposed model of R2 neurons acting upstream of the ExFl2 neurons in the homeostatic regulation of sleep. Signaling from the R2 to ExFl2 neurons is likely indirect, since the pre-synaptic terminals of the R2 neurons are in the ellipsoid body ring while the post-synaptic processes of the ExFl2 neurons are in the dorsal protocerebrum. Although the ExFl2 neurons

are shown as the sole target of R2 signaling, additional downstream sleep "effector" circuits may exist.

(**E**) Sleep profiles of *R72G06-LexA; UAS-dTrpA1* (green diamonds, n=26), *wt>LexAop-TNT*; *R69F08-Gal4>UAS-dTrpA1* (magenta circles, n=44), *R72G06-LexA>LexAop-TNT*; *wt>UAS-dTrpA1* (cyan triangles, n=30), and *R72G06-LexA>LexAop-TNT*; *R69F08-Gal4>UAS-dTrpA1* (black squares, n=34) flies. Sleep time plotted in 30 min bins. White and black bars indicate 12 hr light and dark periods, respectively. 12 hr dTrpA1 activation at 28°C is indicated.

(F) Sleep amount during the 12 hrs after dTrpA1 activation. Data are from the same flies as in **Figure 2E**. Mean ± SEM is shown.

(**G**) Mean GCaMP responses in cell bodies of ExFl2 neurons from *R69F08-Gal4>UAS-P2X2; R72G06-LexA>LexAop-GCaMP6s* (cyan trace, n=6) and *UAS-P2X2; R72G06-LexA>LexAop-GCaMP6s* (black trace, n=5) flies. Black bar denotes time of perfusion 5mM ATP. (See also Figure S2)

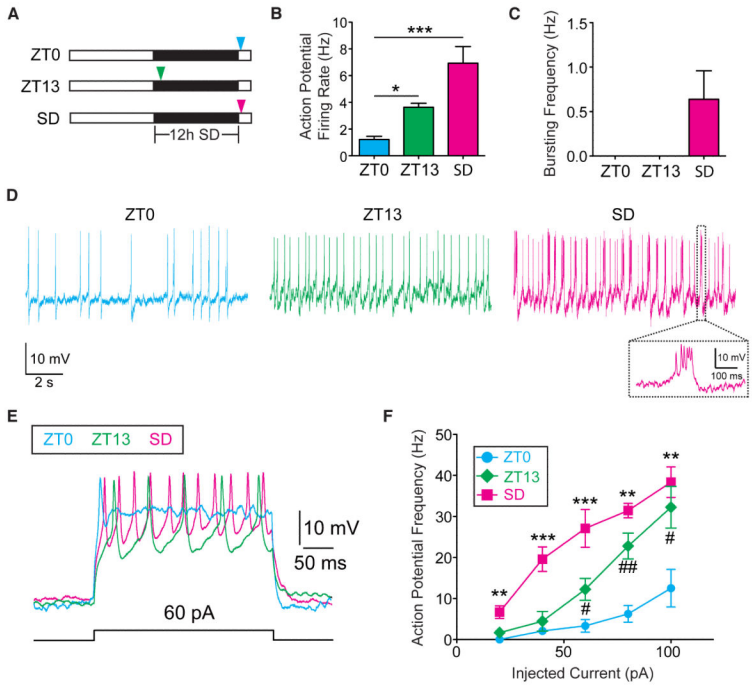

Figure 3.

R2 ring neuron activity and excitability correlate with level of sleep need.

(A) Schematic of the different time points for perforated patch-clamp recordings. Recordings were performed from ZT0-ZT2 (ZT0), ZT13-15 (ZT13), and sleep-deprived flies (SD).

(B) Quantification of spontaneous action potential frequency of the R2 neurons from ZT0 (n=8), ZT13 (n=6) and SD (n=8) flies.

(C) Bursting frequency of the R2 neurons under baseline conditions and following sleep deprivation. Data in **Figures 3B** and **3C** are from the same recordings. Bursting events were not observed in R2 neurons under baseline conditions, whereas they were seen in 6 of 8 recordings from sleep-deprived flies.

(D) Representative whole-cell current-clamp recordings of R2 neurons from ZT0-ZT2, ZT13-ZT15, and following sleep deprivation. Dashed box highlights the bursting event in a sleep-deprived animal.

(E) Representative traces for evoked response to 60 pA current injections. Data from flies at ZT0-ZT2, ZT13-ZT15, and following sleep deprivation are shown in cyan, green, and magenta respectively.

(F) Mean AP frequency evoked in response to current injections with 300-ms stepping pulses at 20 pA increments ranging from 20 pA to 100 pA. Mean ± SEM is shown. (See also Figure S3)

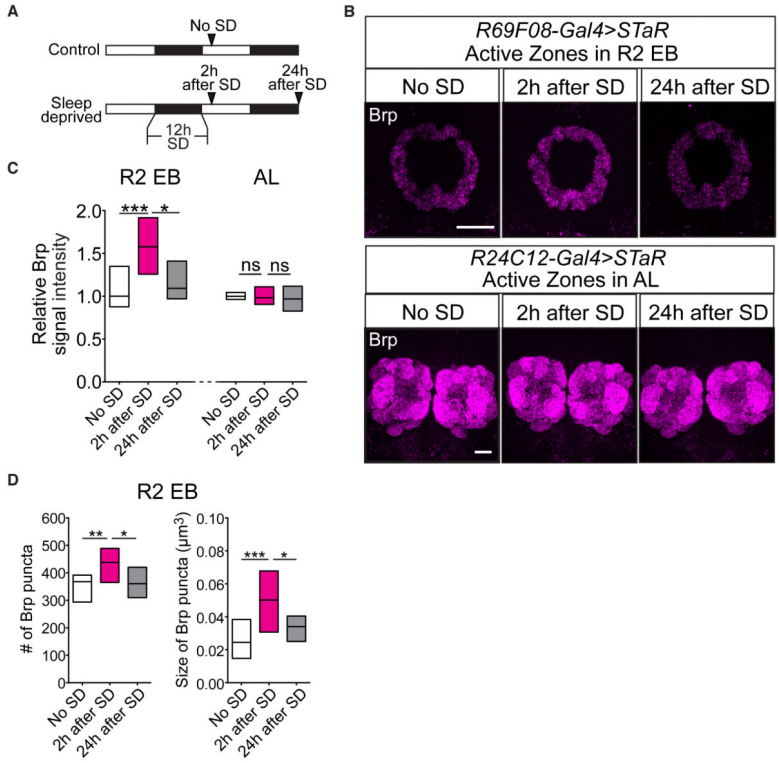

Figure 4.

Structural plastic changes in the R2 circuit correlate with sleep need.

(A) Schematic of the different time points for measurement of BRP, an active zone component.

(B) Representative images of BRP signal in the R2 neurons (*R69F08-Gal4>STaR*, upper panels) and in antennal lobe local interneurons (*R24C12-Gal4>STaR*, lower panels) in No SD, 2 hr after SD and 24 hr after SD flies. Sum intensity projections of the R2 region are shown. Scale bar denotes 20 µm.

(C) Relative levels of BRP signal intensity in the presynaptic region of R2 neurons (R2 EB) in No SD (n=19), 2 hr after SD (n=19) and 24 hr after SD animals (n=16) and relative levels of BRP signal in antennal lobe local interneurons (AL) in No SD (n=10), 2 hr after SD (n=11) and 24 hr after SD animals (n=10). Simplified box plots are shown, where the line inside the box indicates the median, and the top and bottom represent 75% and 25% percentile, respectively.

(D) The number and size of the BRP puncta in the R2 rings in No SD (n=19), 2 hr after SD (n=19) and 24 hr after SD animals (n=16). These data are from the same flies as in **Figure 4C**. (See also Figure S3)

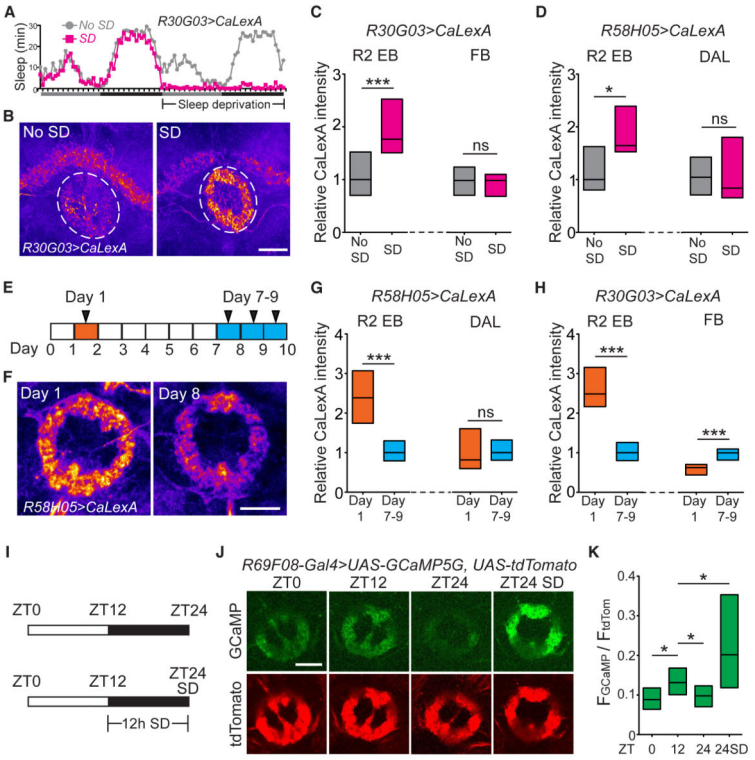

Figure 5.

Intracellular Ca^{2+} within R2 neurons reflects level of sleep drive in scalable manner.

(A) Mechanical sleep deprivation of *R30G03-Gal4>CaLexA* flies. Sleep profiles of flies subjected to “no sleep deprivation” (No SD, gray circles, n=22) or 24 hr sleep deprivation (SD, magenta squares, n=20) are shown. Gray and black bars indicate 12 hr subjective day and night, respectively.

(B) Whole-mount brain immunostaining of SD vs no SD *R30G03-Gal4>CaLexA* flies using anti-GFP. Maximal intensity projections of the central complex region are shown in pseudocolor. Scale bar denotes 20 μm. Dashed lines indicate the R2 ring of the ellipsoid body (EB).

(C) Relative levels of GFP signal in the R2 EB and Fan-shaped body (FB) in No SD and SD flies from **Figure 5A**. Note that the FB neurons in **Figures 5C** and **5H** are not the ExFl2 cells.

(D) Relative levels of GFP signal in R2 EB and dorsal anterior lateral (DAL) neurons in *R58H05-Gal4>CaLexA* flies under No SD (n=10) and SD (n=11) conditions.

(E) Schematic showing the paradigm used for CaLexA measurements in very young (1 day old) vs older (7-9 days old) flies.

(F) Representative whole-mount brain immunostaining of Day 1- vs Day 8-old *R58H05-Gal4>CaLexA* animals. Maximal intensity projections of the R2 ring are shown in pseudocolor. Scale bar denotes 20 μm.

(G) Relative GFP signal in R2 EB and DAL for 1 day old (“Day 1”, n=11) and 7-9 day old (“Day 7-9”, n=10) *R58H05-Gal4>CaLexA* flies.

(H) Relative GFP signal in R2 EB and FB for 1 day old (“Day 1”, n=15) and 7-9 day old (“Day 7-9”, n=10) *R30G03-Gal4>CaLexA* flies.

(I) Schematic of the different time points for real-time Ca^{2+} level measurements using myrGCaMP5G.

(J) Representative images of GCaMP (upper panels) and tdTomato (lower panels) fluorescence intensity in the R2 ring of *R69F08-Gal4>UAS-myrGCaMP5G, UAS-CD4-tdTomato* flies at ZT0, ZT12, ZT24 and ZT24 after 12 hr sleep deprivation (ZT24 SD). Average projections of all the frames in the 1 min recording are shown. Scale bar denotes 20 μm.

(K) Relative GCaMP fluorescence intensity in the R2 ring at ZT0 (n=18), ZT12 (n=15), ZT24 (n=17) and ZT24 SD (n=18). GCaMP fluorescence was normalized to the tdTomato fluorescence signal intensity. Simplified box plots are shown, where the line inside the box indicates the median, and the top and bottom represent 75% and 25%, respectively. (See also Figure S4)

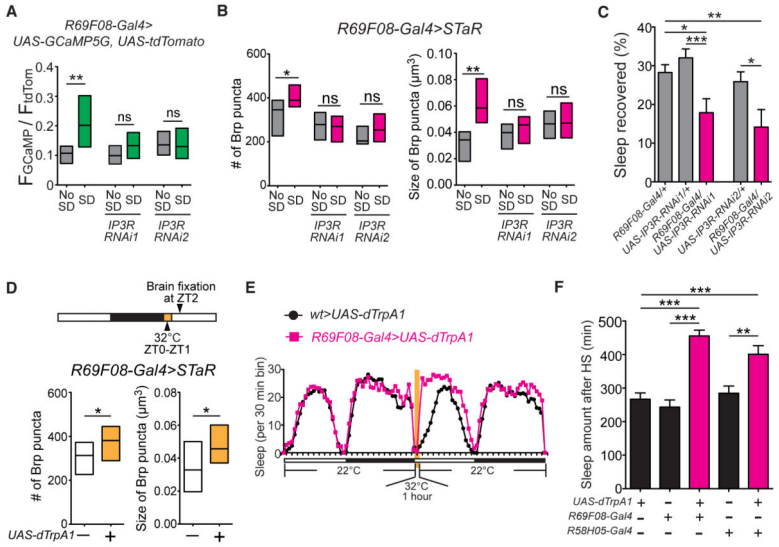

Figure 6.

Manipulating levels of intracellular Ca^{2+}adjusts synaptic strength and amount of sleep drive. **(A)** Relative GCaMP fluorescence intensity in the R2 ring in *R69F08-Gal4>UAS-GCaMP5G*, *R69F08-Gal4>UAS-IP3R-RNAi1, UAS-GCaMP5G*, and *R69F08-Gal4>UAS-IP3R-RNAi2, UASGCaMP5G* flies. Cytosolic Ca^{2+} is increased in control animals after sleep deprivation (n=12 for both No SD and SD), and this increase is blocked in *R69F08-Gal4>UAS-IP3R-RNAi1, UASGCaMP5G* (n=15 for both No SD and SD) and *R69F08-Gal4>UAS-IP3R-RNAi2, UASGCaMP5G* (n=7 for both No SD and SD) animals.

(B) Number and size of BRP puncta in the R2 ring in *R69F08-Gal4>STaR; R69F08-Gal4>UASIP3R-RNAi1, STaR*, and *R69F08-Gal4>UAS-IP3R-RNAi2, STaR* flies. Number and size of BRP puncta are increased in control animals after sleep deprivation (n=13 for No SD and n=13 for SD), and these increases are suppressed in *R69F08-Gal4>UAS-IP3R-RNAi1, STaR* (n=13 for No SD and n=10 for SD) and *R69F08-Gal4>UAS-IP3R-RNAi2, STaR* (n=9 for No SD and n=8 for SD) animals.

(C) % sleep recovered during the first 6 hrs following mechanical sleep deprivation for *R69F08-Gal4>wt* (n=25), *wt>UAS-IP3R-RNAi1*, (n=33), *R69F08-Gal4>UAS-IP3R-RNAi1* (n=27), *wt>UAS-IP3R-RNAi2, UAS-dicer2* (n=24), and *R69F08-Gal4>UAS-IP3R-RNAi2, UAS-dicer2* (n=20) flies.

(D) Upper panel illustrates the paradigm used to elevate Ca^{2+} levels in R2 neurons. Lower panel shows the number and size of BRP puncta in the R2 rings from *R69F08-Gal4>STaR* (n=20) and *R69F08-Gal4>UAS-dTrpA1, STaR* (n=24) flies at ZT2 after a 32°C heat pulse from ZT0-ZT1. Simplified box plots are shown, where the line inside the box indicates the median, and the top and bottom represent 75% and 25%, respectively.

(E) Sleep profile of *wt>UAS-dTrpA1* flies (black circles, n=42) vs *R69F08-Gal4>UAS-dTrpA1* (magenta squares, n=26). Sleep time was plotted in 1 hr bins. White and black bars indicate 12 hr light and dark periods, respectively. 1 hr dTrpA1 activation at 32°C is indicated by the yellow box.

(F) Sleep amount during ZT1-ZT12 following 1 hr dTrpA1 activation. Data from *wt>UAS-dTrpA1* (n=42), *R69F08-Gal4>wt* (n=26), *R69F08-Gal4>UAS-dTrpA1* (n=31), *R58H05-*

Gal4>wt (n=32), and *R58H05-Gal4>UAS-dTrpA1* (n=40) flies are shown. Data for *wt>UAS-dTrpA1* and *R69F08-Gal4>UAS-dTrpA1* are from the same flies as in **Figure 6E**. Mean ± SEM is shown. (See also Figure S5)

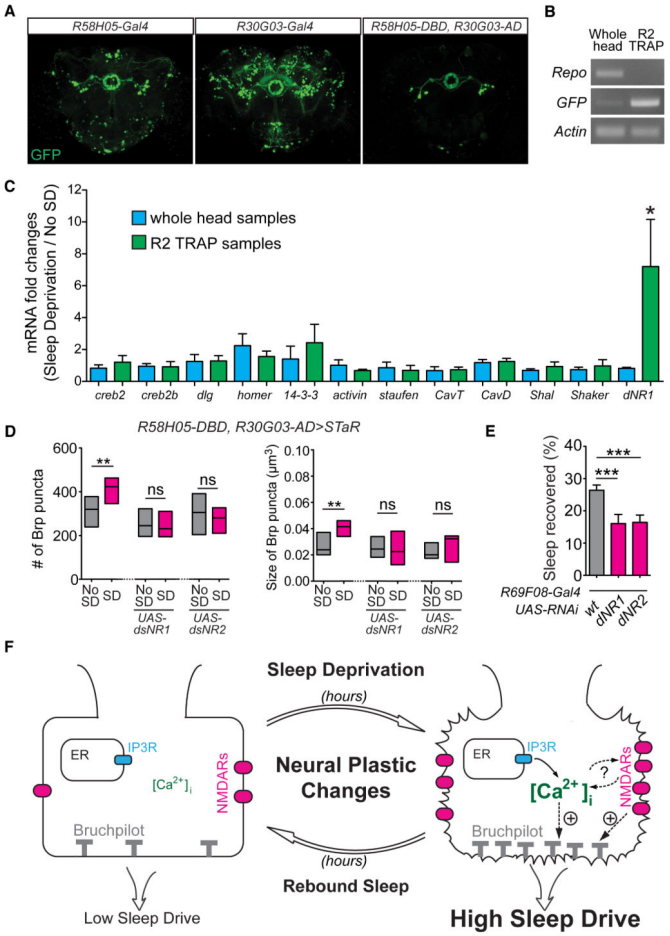

Figure 7.

NMDA receptor expression in the R2 circuit is required for sleep need-dependent plasticity and generation of homeostatic sleep drive.

(A) Whole-mount brain immunostaining of *R58H05-Gal4>UAS-IVS-Syn21-GFP-p10*, *R30G03-Gal4>UAS-IVS-Syn21-GFP-p10* and *R58H05-DBD, R30G03-AD>UAS- IVS-Syn21-GFP-p10* animal with anti-GFP. Maximal intensity projection of the central brain is shown.

(B) Representative RT-PCR for *Repo*, *GFP*, and *actin* from whole brain samples and R2 TRAP samples. For detecting *Repo* and *actin*, 30 cycles were used. For detecting *GFP* signal, 42 cycles were used.

(C) Relative change in mRNA levels between sleep-deprived and non-sleep-deprived (no SD) animals from whole brain (cyan bars) or R2 TRAP (green bars) samples. Data from 12 different neural plasticity-related genes: *creb2* (n=3), *creb2b* (n=3), *dlg* (n=3), *homer* (n=3), *14-3-3* (n=3), *activin* (n=3), *staufen* (n=3), Ca_VT (n=3), Ca_VD (n=3), *Shal* (n=3), *Shaker* (n=3), and *dNR1* (n=4) are shown.

(D) Number and size of BRP puncta in the R2 ring in R58H05-DBD, R30G03-AD>STaR, R58H05-DBD, R30G03-AD >UAS-dsNR1, STaR, and *R58H05-DBD, R30G03-AD>UAS-dsNR2, STaR* flies. Number and size of BRP puncta are increased in control animals after sleep deprivation (n=11 for No SD and n=11 for SD), and these increases are blocked in

R58H05-DBD, R30G03-AD>UAS-dsNR1, STaR (n=12 for No SD and n=13 for SD) and *R58H05-DBD, R30G03-AD>UAS-dsNR2, STaR* (n=8 for both No SD and SD) animals.
(E) % sleep recovered during the first 6 hrs following mechanical sleep deprivation for *R69F08-Gal4>UAS-dicer2* (n=59), *R69F08-Gal4>UAS-dsNR1, UAS-dicer2* (n=37) and *R69F08-Gal4>UAS-dsNR2, UAS-dicer2* (n=34) flies.
(F) Proposed model illustrating the encoding of sleep drive in R2 neurons. Following hours of sleep deprivation, R2 neurons exhibit an IP3R-dependent increase in cytosolic Ca2+ levels and a marked increase in NMDA receptor levels. These changes lead to both electrical potentiation of the R2 neurons, and increased synaptic strength of these neurons, as indicated by higher levels of BRP. Sleep drive is encoded by the persistently increased synaptic strength of the R2 circuit and is maintained for hours following restoration of sleep. (See also Figure S6)